Eur. Phys. J. B **61**, 433–439 (2008)
DOI: 10.1140/epjb/e2008-00104-3

THE EUROPEAN PHYSICAL JOURNAL B

Structural dependence of exciton in carbon nanotubes

Y. Jia, G. Yu, and J. Dong[a]

Group of Computational Condensed Matter Physics, National Laboratory of Solid State Microstructures and Dept. of Physics, Nanjing University, Nanjing 210093, P.R. China

Received 20 August 2007 / Received in final form 31 December 2007
Published online 13 March 2008 –

Abstract. The binding energies and sizes of excitons, and energy splitting of the bright-dark excitons in single-walled carbon nanotubes have been calculated using the nonorthogonal tight-binding model, supplemented by the long-range Coulomb interaction. It is found that the binding energies and the sizes of excitons not only depend on tube's diameter d, but also its chirality. However, the splitting of the bright-dark excitons mostly depends on $1/d^2$. Our obtained results show that the curvature effect is very important for the exciton excitations in the SWNTs, especially in the smaller diameter ones.

PACS. 78.67.Ch Nanotubes – 73.22.-f Electronic structure of nanoscale materials: clusters, nanoparticles, nanotubes, and nanocrystals – 71.35.-y Excitons and related phenomena

1 Introduction

Carbon nanotubes (CNTs) have attracted much attention theoretically and experimentally in recent years due to their unique geometrical, electronic and optical properties [1]. The single-walled carbon nanotubes (SWNTs) can be viewed as a long strip of graphene sheet rolled up into a seamless cylindrical surface. Their structures can be characterized by a pair of integers, (n, m), which determines their diameters and chiralities [2].

The CNT's optical properties are of great importance because of their potential applications in future nanoscale optoelectronics [3,4]. And a number of groups have studied their optical absorption and emission spectra [5–11], among which the initial theoretical works often used the single-electron theory to explain the experimental observations [5]. However, recent experiments and theoretical calculations on the CNT's optical spectra suggest that the exciton effect dominates their optical absorption and emission [12–16]. Because of the strong quantum confinement of electron and hole in the quasi-one-dimensional structures of CNTs, the large binding energies of excitons can be expected [17], which have been confirmed by the recent experiments based on two-photon spectroscopy, showing an anomalously large value equal to a substantial fraction of the band gap [18,19].

Therefore, a number of theoretical approaches have been used to calculate the binding energies of CNT's excitons. One approach is the variational calculation, which, while valuable, cannot give the spectral weight [20]. The more accurate calculation is the solution of Bethe-Salpeter equation using the GW-corrected quasiparticle energies, which employs the ground state obtained by an ab initio approach [14]. But this approach is difficult to implement for the chiral SWNTs with many atoms in a unit cell. So, the semi-empirical method based on π -electron approximation has been used for a larger variety of CNTs [16–21], in which, however, the curvature-induced $\sigma - \pi$ mixing was not included. As well known, the $\sigma - \pi$ hybridization can change significantly the electronic structures of CNTs with small diameters. For instance, the band gap in small-radius CNTs can be reduced down to 50%, compared to that obtained by the π- orbital only tight-binding (TB) model, which is caused by the strong curvature-induced $\sigma - \pi$ hybridization [22]. Obviously, the $\sigma - \pi$ mixing will have a big effect on the exciton binding energy in the small-diameter CNTs.

So, in this paper, we have studied the curvature effects on the exciton binding energy in the SWNTs by using the symmetry-adapted nonorthogonal TB (SA-NTB) model [23], including the long-range Coulomb interaction [24]. It allows us to use a two-atom unit cell instead of the translational primary unit cell of the SWNTs, in which thousands of atoms could be contained for a chiral SWNT. The obtained results show that the exciton binding energies depend strongly on both diameters and chiralities of the SWNTs, which are well consistent with the experimental observations. In addition, a comparison of our obtained results with those from the simple π-electron TB model has been made, from which a more distinct dependence of the exciton binding energy on the SWNT chirality is found.

The paper is organized as follows. In Section 2, the SA-NTB model and the standard exciton theory are

[a] e-mail: jdong@nju.edu.cn

introduced. The results and discussions are presented in Section 3. And the conclusions are given in Section 4.

2 Model and method

The SA-NTB model has been used to calculate the band structures of SWNTs [23] and their resonant Raman intensity of the radial breathing mode (RBM) [26]. In this model, a two-atom unit cell is used instead of the translational primary unit cell. And the electron's wave function $\psi_{kl}(\mathbf{r})$ can be expanded as a linear combination of the atomic orbitals in the two-atom unit cell.

$$\psi_{kl}(\mathbf{r}) = \sum_r a_{klr}\varphi_{klr}(\mathbf{r}). \tag{1}$$

Here, $-\pi/T \le k < \pi/T$ and $l = 0, 1, \ldots, N_c - 1$, with T the 1D translational period of CNT and N_c the number of hexagons in a translational primary unit cell of CNT. a_{klr} is the expansion coefficient. The index r runs over the orbitals of two atoms in the two-atom unit cell.

The one-electron Hamiltonian of a SWNT can be written as

$$H_0 = -\frac{\hbar^2\nabla^2}{2m} + V(r). \tag{2}$$

Here m is the electron's mass. And $V(r)$ is the effective periodic potential.

From the one-electron Schödinger equation, $H_0\psi_{kl}(r) = E_{kl}\psi_{kl}(r)$, one can obtain the matrix equation for the coefficients a_{klr}

$$\sum_{r'}(H_{klrr'} - E_{kl}S_{klrr'})a_{klr'} = 0. \tag{3}$$

Here $H_{klrr'}$ and $S_{klrr'}$ are the matrix elements of the one-electron Hamiltonian H_0 and the overlap matrix S, respectively. And E_{kl} is the one-electron energy. From equation (3), we can obtain the electron energies E_{klr} and the expansion coefficients $a_{klrr'}$, $r = 1, 2, \ldots, 2p$. Here $2p$ is the number of atomic orbitals in the two-atom unit cell ($p = 1$ for the π-band TB model, and $p = 4$ for the $\sigma - \pi$ coupling TB model). In the usual orthogonal TB models, the overlap of the atomic orbitals centered on different atoms is ignored, and so the $S_{klrr'}$ becomes a unit matrix.

We perturb the one-electron Hamiltonian with the π-orbital only electron-electron Coulomb interaction Hamiltonian H_{e-e}, which can be described as follows:

$$H_{e-e} = U\sum_i n_{i\uparrow}n_{i\downarrow} + \frac{1}{2}\sum_{i\neq j} V_{ij}(n_i - 1)(n_j - 1). \tag{4}$$

Here, $n_{is} = C_{is}^\dagger C_{is}$ is the number of π electrons with spin s on the ith atom, and $n_i = \sum_s n_{is}$ is the total number of π electrons on the ith atom. The $C_{is}^\dagger(C_{is})$ is creation (annihilation) operator of electron at the ith site with spin s. The parameter U is the on-site Coulomb interaction between two π-electrons occupying the p_z orbital of the same carbon atom, and V_{ij} is the inter-site e-e interaction. In the actual calculations, the long-range Coulomb interaction V_{ij} is parameterized by the Ohno formula [25]:

$$V_{ij} = \frac{U}{\kappa\sqrt{1 + 0.6117r_{ij}^2}}. \tag{5}$$

Here, r_{ij} is the distance between carbon atoms i and j in a unit of Å, and κ is introduced to take into account the dielectric screening effect of the medium. In this paper, the parameters U and κ are taken to be 8.0 eV and 2, respectively [21].

According to the standard exciton theory [24], we first obtain the single electron state of H_0, and then construct the ground state $\mid g >$ and the excited state of a single electron-hole pair. The matrix of the Hamiltonian $H = H_0 + H_{e-e}$ can be calculated and diagonalized numerically within the single-excitation subspace. Here, we have used the periodic boundary condition to assure that the total momentum of a single excitation is a good quantum number.

Let us consider a single electron-hole pair excitation, in which an electron with wave number $\mathbf{k}_v$ in a state of the valence band ($v = klm$) is promoted to a state of the conduction band with wave number $\mathbf{k}_c$ ($c = klm'$). Note that the quantum number k is discrete because of the finite length effect of the SWNTs, which is equal to $k = \frac{2\pi j}{LT_0}$ (j is an integer number,$-L/2 \le j < L/2$). Here L is the number of the translational primary unit cells with its length of T_0 in the SWNT. Then the single electron-hole excited state can be constructed from the ground state $\mid g >$ as follows,

$$\mid \mathbf{k}_c, \mathbf{k}_v\rangle = \frac{1}{\sqrt{2}}(C_{\mathbf{k}_c\uparrow}^\dagger C_{\mathbf{k}_v\uparrow} \pm C_{\mathbf{k}_c\downarrow}^\dagger C_{\mathbf{k}_v\downarrow}) \mid g\rangle. \tag{6}$$

Here, "+" represents the spin singlet and "−", the spin triplet. In general, we introduce new variables $\mathbf{k}$ and $\mathbf{K}$, defined as follows:

$$\mathbf{k}_c = \mathbf{k} + \mathbf{K}, \quad \mathbf{k}_v = \mathbf{k} - \mathbf{K}. \tag{7}$$

And denote the excited state as $\mid \mathbf{k}, \mathbf{K} >$. Here $\mathbf{k}$ and $2\mathbf{K}$ are the relative and the center-mass momentum of the electron-hole pair, respectively. The matrix elements of the excitation Hamiltonian in this representation can be written as [24,27]

$$\begin{aligned}\langle \mathbf{k}', \mathbf{K}'|(H - E_0)|\mathbf{k}, \mathbf{K}\rangle = \delta_{\mathbf{K}',\mathbf{K}}\{\delta_{\mathbf{k}',\mathbf{k}}[\tilde{\epsilon}_c(\mathbf{k}+\mathbf{K}) - \tilde{\epsilon}_v(\mathbf{k}-\mathbf{K})] \\ + 2\delta_S W_X(\mathbf{k}', \mathbf{k}; \mathbf{K}) - W_C(\mathbf{k}', \mathbf{k}; \mathbf{K})\}\end{aligned} \tag{8}$$

for spin singlet ($\delta_S = 1$) and triplet ($\delta_S = 0$) states. Here $E_0 = \langle g|H|g\rangle$ is the ground-state energy. The quantities $\tilde{\epsilon}_c$ and $\tilde{\epsilon}_v$ are the one-electron energies in the conduction and the valence bands, respectively, which include the first-order energy corrections with respect to the interaction. W_C and W_X represent the direct Coulomb part and the exchange part, respectively. They can be expressed by the

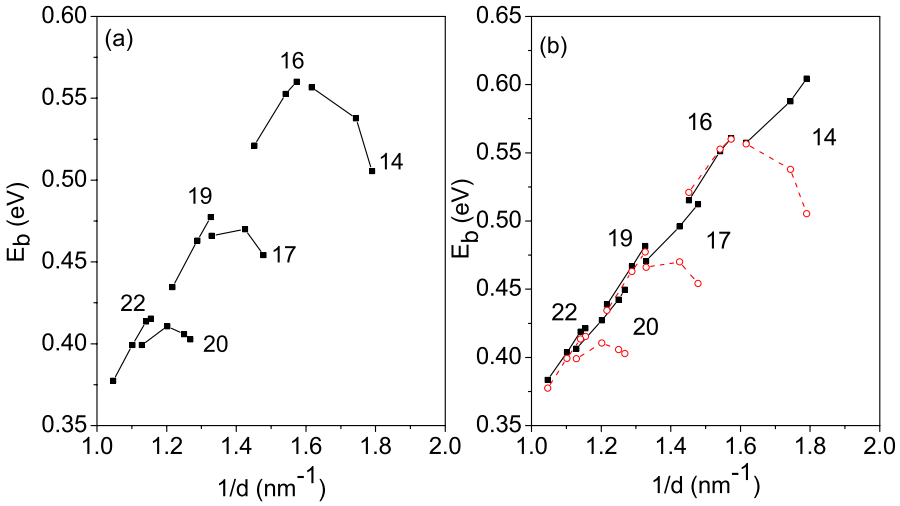

Fig. 1. (color online) Binding energies of the E_{11} bright excitons versus $1/d$, calculated within: (a) the SA-NTB model, and (b) the simple π-TB model. For comparison, in (b) is also given the values got from the SA-NTB model, which are represented by the red open circles. In both of (a) and (b), the numbers indicate the $(2n+m)$ family indices. Within a branch, the indices of two neighboring tubes are related by $(n', m') = (n-1, m+2)$ For example, when $2n+m=14$, the nanotube indices are (7, 0), (6, 2), (5, 4) with their diameters increased.

coefficients of one-electron wave functions:

$$W_C(\mathbf{k}', \mathbf{k}; \mathbf{K}) = \frac{1}{N_u} \sum_{u=1}^{N_u} \sum_{r,r'=A,B} e^{i(\mathbf{k}-\mathbf{k}')\bullet(\mathbf{R}_{u,r}-\mathbf{R}_{0,r'})} \times V(|\mathbf{R}_{u,r} - \mathbf{R}_{0,r'})a_r^{c*}(\mathbf{k}' + \mathbf{K})a_r^c(\mathbf{k} + \mathbf{K})a_{r'}^v(\mathbf{k}' - \mathbf{K}) \times a_{r'}^{v*}(\mathbf{k} - \mathbf{K}),$$

$$W_X(\mathbf{k}', \mathbf{k}; \mathbf{K}) = \frac{1}{N_u} \sum_{u=1}^{N_u} \sum_{r,r'=A,B} e^{2i\mathbf{K}\bullet(\mathbf{R}_{u,r}-\mathbf{R}_{0,r'})} \times V(|\mathbf{R}_{u,r} - \mathbf{R}_{0,r'})a_r^{c*}(\mathbf{k}' + \mathbf{K})a_{r'}^c(\mathbf{k} + \mathbf{K})a_r^v(\mathbf{k}' - \mathbf{K}) \times a_{r'}^{v*}(\mathbf{k} - \mathbf{K}). \quad (9)$$

Here A and B represent the two atoms in the two-atom unit cell. And N_u is the number of the two-atom unit cells in the SWNT. The superscript c and v represent the conduction and valence band respectively.

If the system has spatial inversion symmetry, such as zigzag nanotubes, the singlet and triplet states can be divided into two types of states: symmetric A_g state and antisymmetric B_u one.

3 Results and discussions

The parameters of the SA-NTB model were taken from a study based on the density functional method [28], showing an excellent performance in the calculation of the equilibrium lattice and the cohesive energy of graphite [23]. According to optical selection rules, only singlet excitons are the optically active ones. In this paper, the exciton binding energies are calculated at $\mathbf{K} = 0$. For zigzag semiconducting SWNTs, the tube length is taken to be 200 T_0, and for chiral semiconducting ones, the tube length is 40 T_0.

We calculate the binding energies of optical active excitons for 20 SWNTs by the SA-NTB model, supplemented by the long range Coulomb interactions. The calculated binding energies of E_{11} bright excitons are given in Figure 1a as a function of the inverse diameters $1/d$, in which the $(2n+m)$ family indices are also indicated. It is found from Figure 1a that the exciton binding energies depend on both the tube's diameter and the value of $\nu =$ mod $(2n+m, 3)$. It is seen clearly that for the SWNTs with their $\nu =$ mod $(2n+m, 3) = 1$(mod1), the exciton binding energies could be well fitted by $E_b = \frac{\alpha}{d}$, which does not hold for the SWNTs with $\nu =$ mod $(2n+m, 3) =$ 2(mod2). In addition, the exciton binding energies of the mod1 SWNTs are greatly larger than those of the mod2 SWNTs with the same diameters. The obtained results are in agreement with the conclusions of a symmetry-based variational method [20]. And this family pattern is very similar to the so-called Kataura plots for the optical transition energies E_{11} [5].

For comparison, we have shown in Figure 1b the binding energies of bright excitons calculated from both the simple TB and the SA-NTB models. In the simple TB model, the nearest-neighbor hopping parameter t_0 is chosen to be -2.0 eV, which has been used successfully in reference [21]. We can see that the binding energy of E_{11} bright exciton got from the simple TB model depends mostly on tube's diameters, but very weakly on their chiral angles. So, the E_{11} exciton binding energy of all SWNTs, no matter mod1 or mod2 ones, can be fitted approximately

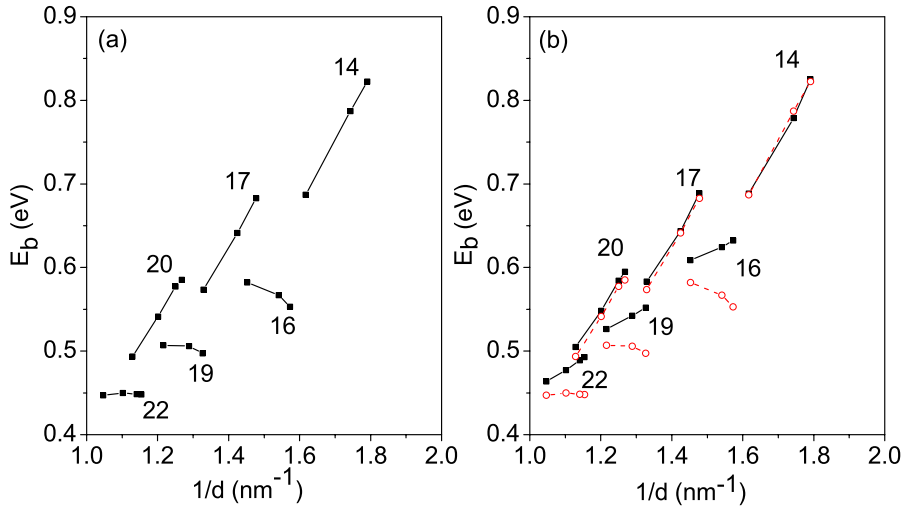

Fig. 2. The same as Figure 1, but now for E_{22} bright excitons.

by

$$E_b = \frac{\alpha}{d}. \tag{10}$$

Here, the coefficient α is found to be 0.35 eV nm for the E_{11} bright excitons, which is consistent with previous theoretical calculations [21]. And it can also be seen clearly from Figure 1b that the discrepancy between two calculated results is different for mod1 and mod2 SWNTs, which is particularly obvious for the smaller diameter SWNTs. For the mod2 nanotubes, there is a large discrepancy between the two calculated results. The maximum discrepancy occurs in the zigzag-like tubes, but the minimum one in the close-to-armchair tubes, i.e., the discrepancy increases with decreasing chiral angles. However, such a strong discrepancy between the two calculations is not seen in the mod1 nanotubes. The obvious difference between the calculated results from two TB models indicates that the curvature effect brings the great modifications in the family patterns, especially for the narrow nanotubes. And the calculation based on the simple TB model is not sufficient for describing the large family behavior.

In Figure 2a, we have plotted the binding energies of E_{22} bright excitons against the inverse tube diameter, obtained from the SA-NTB model. The results shown in Figure 2a indicate that the E_{22} bright excitons of mod2 nanotubes have the larger binding energies than those of mod1 nanotubes with similar diameters, which is completely different from that shown in Figure 1a for the E_{11} bright excitons. And the family pattern is also similar to the Kataura plot for the E_{22} optical transitions. When compared with the E_{11} bright excitons, we can find that the binding energy of E_{22} bright exciton is generally greater than that of E_{11} bright exciton except for the mod1's (8, 0) nanotube [20,27].

In Figure 2b, we have made a comparison of binding energies of E_{22} bright excitons obtained from two different TB models. It is seen from Figure 2b that although the binding energies of E_{22} bright excitons, calculated in the simple TB model, have a larger dependence on tube chirality than those of E_{11} bright excitons, they can still be fitted by equation (10), but with a different α coefficient of 0.43 eV nm, which is remarkably close to the previous theoretical result, $E_b = \frac{0.42}{d}$ eV [21]. And we also compare our results with the theoretical ones obtained by solving the Bethe-Salpeter equation within TB model, finding that the variation of exciton binding energies with $1/d$ in the two calculations is similar to each other. From Figure 2b, we find a very good match between the calculated results within the two TB models for the mod2 nanotubes. But for the mod1 nanotubes, the results calculated within the SA-NTB model deviate systematically from those obtained by the simple TB model. Within the same $(2n + m)$ family, this deviation increases with decreasing chiral angle for mod1 nanotubes.

From our calculations, it is found that both the binding energies of E_{11} and E_{22} excitons show the family behavior, which can be understood from the trigonal warping effect [27]. And from Figures 1b and 2b, it is clear seen that the E_{ii} exciton binding energies calculated within the SA-NTB model deviate systematically from those got from the simple TB model for the branches on the lower-energy side of the exciton binding energies. This deviation increases for the SWNTs with smaller chiral angels within the same $(2n + m)$-family (similar d), and would become weaker for large diameter tubes. This chiral-angle dependent deviation is due to the modification of the electronic structure by the curvature-induced rehybridization of σ and π bands, which is stronger for the states lying between the K and M point of the Brillouin zone (BZ) of graphite, and weaker for the states from the other sides of the K point [29]. In semiconducting tubes, the E_{11} optical transitions for mod1 and mod2 SWNTs take place along the ΓK and KM line, respectively, in the BZ of graphene, while the situation becomes just reverse for the E_{22} optical

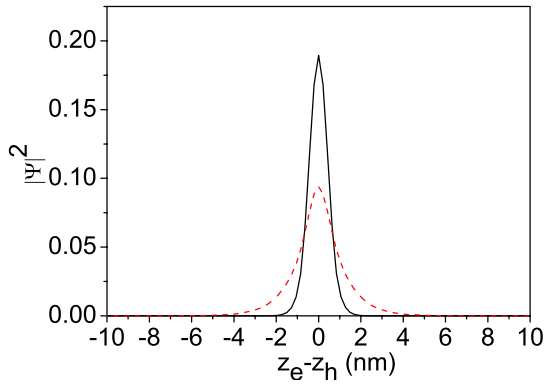

Fig. 3. (color online) The lowest-energy bright exciton's wave functions of the (7, 0) nanotube, averaged along the circumference direction. Black solid and red dashed lines denote the E_{22} and E_{11} bright excitons, respectively.

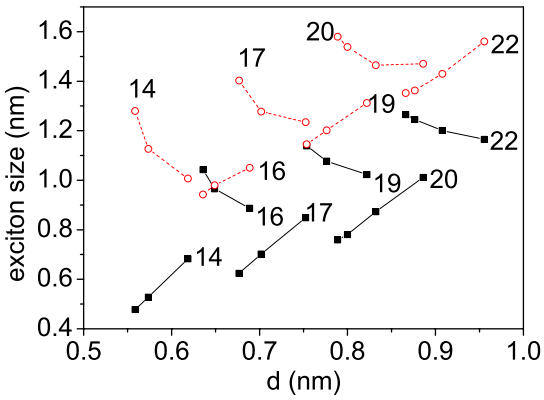

Fig. 4. (color online) Bright exciton's sizes of 20 SWNTs versus tube's diameter. Black filled squares and red open circles denote the E_{22} and E_{11} bright excitons, respectively. The labels indicate the $(2n + m)$ family indices.

transitions. So, for the E_{11} optically active excitons, the difference between the calculated results from two models is larger for mod2 nanotubes than that for mod1 nanotubes. But, for the E_{22} optically active excitons, the result is reversed: the difference in mod1 nanotubes is larger than that in mod2 ones. Within the same $(2n + m)$ family, the maximum effect of the $\sigma - \pi$ hybridization occurs for zigzag nanotubes, and the minimum one for closed-to-armchair nanotubes. Therefore, the difference decreases with increasing the chiral angle.

From Figures 1b and 2b, it is found that at the same chiral angle, the discrepancy between the calculated results from different TB models depends on tube's diameter, which decreases with increasing the tube's diameter. For example, the discrepancies for E_{11} optical active excitons in (7, 0) and (10, 0) SWNTs are 99 and 47 meV, respectively. So, for the small diameter SWNTs ($d < 1.0$ nm), the curvature effect is very important, making the simple TB model insufficient to describe the optical properties of SWNTs [27,30].

It is known that the binding energy can be reflected from the exciton's wave function or the exciton size. In Figure 3, we show the wave functions $\psi(r_e, r_h)$ of the lowest-energy E_{11} and E_{22} bright excitons for the (7, 0) SWNT, which are obtained within the SA-NTB model and averaged over the coordinates perpendicular to the tube. It is seen from Figure 3 that the wave function of the E_{11} bright exciton is less localized along the tube axis than that of the E_{22} one. That is why the E_{22} bright exciton has a larger binding energy than the E_{11} one for the (7, 0) nanotube.

The exciton size along the tube axis can be obtained from the formula, $\chi = \sqrt{\langle (z_e - z_h)^2 \rangle}$. We have calculated the exciton sizes of the E_{11} and E_{22} bright excitons for 20 SWNTs within the SA-NTB model. The obtained results, varying with tube's diameter, are shown in Figure 4. Again, as expected, the exciton sizes increase with tube's diameter and also show the $(2n + m)$-family behaviors. For the E_{11} bright excitons, the mod2 SWNTs have larger exciton sizes than the mod1 SWNTs. While for the E_{22} bright excitons, the situation becomes reversed, i.e., the mod1 SWNTs have larger exciton sizes than the mod2 ones. From Figure 4, we can also see that the E_{11} bright excitons always have the larger sizes than the E_{22} ones except for the (8, 0) nanotube. The family behavior of the exciton sizes can be also understood from the trigonal warping effect and the tube curvature effects. And the anomalous behavior in the exciton size of (8, 0) nanotube indicates once again the importance of the curvature effect, especially for the narrow nanotubes.

We have also studied the diameter- and chirality-dependence of the energy splitting between the E_{11} bright and dark excitons. According to the selection rule of photon absorption for exciton in SWNTs, the triplet exciton is optically forbidden. The lowest-energy exciton is a triplet one, and so it is optically inactive. The energy splitting δ between the lowest-energy exciton and the bright exciton calculated within the simple TB model is given in Figure 5a, showing an inverse proportion to the square of tube's diameter:

$$\delta = \frac{\gamma}{d^2}. \tag{11}$$

Here, the coefficient γ is found to be 26.94 eV nm^2. However, our calculated splitting from the SA-NTB model, given in Figure 5b, shows the clear family behavior, i.e., the linear dependence of the splitting on $1/d^2$ only holds for the mod1 SWNTs with its coefficient γ being 26.77 meV nm^2, but not for the mod2 SWNTs, which is particularly obvious for narrow tubes. So, we think the curvature effect on the splitting of narrow SWNTs is also of great importance.

Finally, we would like to compare our results from the SA-NTB model with the experimental results. In our calculations, we introduce the dielectric constant κ to describe the environmental or screening influence. We find that the exciton binding energies follow very nicely the scaling $E_b \propto \kappa^{-\alpha}$, which has been predicted by previous theoretical work [15]. Our calculations found the coefficient α is $\alpha \cong 1.44$. Therefore, we can adjust the dielectric

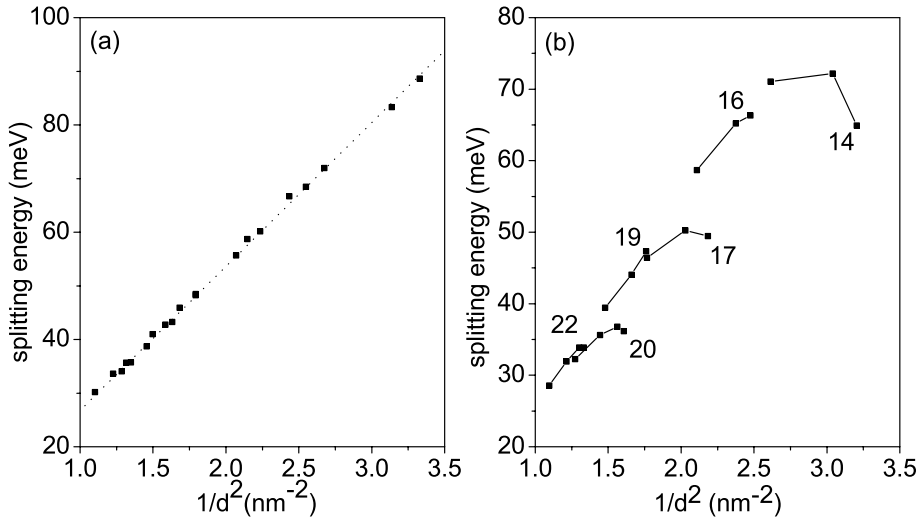

Fig. 5. (a) Energy splitting between bright and dark excitons vs. $1/d^2$, calculated within the simple π-TB model. The dotted line is the linear fit. (b) The same plot as (a), but now calculated within the SA-NTB model. The labels indicate the $(2n+m)$ families.

constant κ to match our calculation results to the experimental data. For example, when we choose $\kappa = 2.25$, the exciton binding energies can be in an excellent agreement with the experimental data in reference [13] for eight SWNTs with $d < 1.0$ nm. The average error is less than 0.02 eV. Similarly, the results of Maultzsch et al. [31] for six different SWNTs are reproduced with a standard deviation of 0.02 eV by using a slightly smaller dielectric constant $\kappa = 2.2$. So, our calculation results obtained by the SA-NTB model can be well consistent with experimental data.

In another experiment, Raman spectroscopy under electrochemical doping was used in nanotubes coated with a surfactant, giving (0.62±0.05) eV and (0.49±0.05) eV for the binding energies of excitons associated with E_{22} transition in (7, 5) and (10, 3) SWNTs, respectively [32]. We have also calculated the binding energies of those excitons. By using $\kappa = 1.85$, the exciton binding energies calculated within the SA-NTB model are 0.58 eV for the (7, 5) tube and 0.53 eV for the (10, 3) tube, which are well consistent with experimental results.

On the other hand, we have compared our results with ab initio ones obtained from solving the Bethe-Salpeter equation [11]. For (8, 0) nanotube in Reference [11], the excitation energies for E_{11} and E_{22} states are found to be 1.55 and 1.80 eV, respectively. The corresponding energy ratio is $E_{22}/E_{11} = 1.16$. The exciton binding energies for E_{11} and E_{22} states are 0.99 eV and 0.86 eV, respectively. In our calculations, when we choose $\kappa = 1.2$, the excitation energies for E_{11} and E_{22} states are 1.56 and 1.89 eV, respectively, and correspondingly $E_{22}/E_{11} = 1.21$. The calculated exciton binding energies for the E_{11} and E_{22} states from the SA-NTB model are 1.02eV and 1.00 eV, respectively. It is seen that our results are consistent with the ab initio results.

4 Conclusions

In summary, we have calculated the binding energies and sizes for the E_{11} and E_{22} bright exciton using the standard exciton theory within both the simple and the nonorthogonal TB models. It is found that the exciton binding energies and sizes calculated within the nonorthogonal TB model have shown a strong diameter- and chirality-dependence, and a distinct family behavior. Comparison between the calculated results within the two TB models indicates that the curvature effects are important, changing significantly the exciton binding energies and their sizes. Finally, we have also found that the energy splitting of the bright-dark excitons is inversely proportional to the square diameter ($\sim 1/d^2$).

This work was supported by the Natural Science Foundation of China under Grant No. 90503012, and also from a Grant for State Key Program of China through Grant No. 2004CB619004 and 2006CB921803.

References

1. M.S. Dresselhaus, G. Dresselhaus, Ph. Avouris, *Carbon nanotubes: Synthesis, Structure, Properties, and Applications* (Springer-Verlag, Berlin, 2001)
2. R. Saito, G. Dresselhaus, M.S. Dresselhaus, *Physical Properties of Carbon Nanotubes* (Imperial College Press, London, 1998)
3. J.A. Misewich, R. Martel, Ph. Avouris, J.C. Tsang, S.Heinze, J. Tersoff, Science **300**, 783 (2003)
4. T. Hertel, G. Moos, Phys. Rev. Lett. **84**, 5002 (2000)
5. S.M. Bachilo, M.S. Strano, C. Kittrell, R.H. Hauge, R.E. Smalley, R.B. Weisman, Science **298**, 2361 (2002)

6. M.J. O'Connell, S.M. Bachilo, X.B. Huffman, V.C. Moore, M.S. Strano, E.H. Haroz, K.L. Rialon, P.J. Boul, W.H. Noon, C. Kittrell, J. Ma, R.H. Hauge, R.B. Weisman, R.E. Smalley, Science **297**, 593 (2002)
7. A. Hagen, T. Hertel, Nano. Lett. **3**, 383 (2003)
8. Z.M. Li, Z.K. Tang, H.J. Liu, N. Wang, C.T. Chan, R. Saito, S. Okada, G.D. Li, J.S. Chen, N. Nagasawa, S. Tsuda, Phys. Rev. Lett. **87**, 127401 (2001)
9. S. Lebedkin, F. Hennrich, T. Skipa, M.M. Kappes, J. Phys. Chem. B **107**, 1949 (2003)
10. J. Lefebvre, Y. Homma, P. Finnie, Phys. Rev. Lett. **90**, 217401 (2003)
11. C.D. Spataru, S. Ismail-Beigi, L.X. Benedict, S.G. Louie, Phys. Rev. Lett. **92**, 077402 (2004)
12. T.Ando, J. Phys. Soc. Jpn. **66**, 1066 (1997)
13. E. Chang, G. Bussi, A. Ruini, E. Molinari, Phys. Rev. Lett. **92**, 196401 (2004)
14. G. Yu, Y. Jia, J. Dong, Phys. Rev. B **76**, 125403 (2007)
15. V. Perebeinos, J. Tersoff, P. Avouris, Phys. Rev. Lett. **92**, 257402 (2004)
16. H. Zhao, S. Mazumdar, Phys. Rev. Lett. **93**, 157402 (2004)
17. R. Loudon, Am. J. Phys. **27**, 649 (1959)
18. F. Wang, G. Dukovic, L.E. Brus, T. Heinz, Science **308**, 838 (2005)
19. G. Dukovic, F. Wang, D.H. Song, M.Y. Sfeir, T.F. Heinz, L.E. Brus, Nano. Lett. **5**, 2314 (2005)
20. R.B. Capaz, C.D. Spataru, S. Ismail-Beigi, S.G. Louie, Phys. Rev. B **74**, 121401(R) (2006)
21. Z.D. Wang, H.B. Zhao, S. Mazumdar, Phys. Rev. B. **74**, 195406 (2006)
22. X. Blase, L.X. Benedict, E.L. Shirley, S.G. Louie, Phys. Rev. Lett. **72**, 1878 (1994)
23. V.N. Popov, New J. Phys. **6**, 17 (2004)
24. S. Abe, J. Yu, W.P. Su, Phys. Rev. B **45**, 8264 (1992)
25. K. Ohno, Theor. Chim. Acta **2**, 219 (1964)
26. V.N. Popov, L. Henrard, Ph. Lambin, Nano. Lett. **4**, 1795 (2004)
27. J. Jiang, R. Saito, Ge. G. Samsonidze, A. Jorio, S.G. Chou, G. Dresselhaus, M.S. Dresselhaus, Phys. Rev. B **75**, 035407 (2007)
28. D. Porezag, Th. Frauenheim, Th. Köhler, G. Seifert, R. Kaschner, Phys. Rev. B **51**, 12947 (1995)
29. S. Reich, C. Thomsen, P. Ordejón, Phys. Rev. B **65**, 155411 (2002)
30. S. Reich, J. Maultzsch, C. Thomsen, P. Ordejón, Phys. Rev. B **66**, 035412 (2002)
31. J. Maultzsch, R. Pomraenke, S. Reich, E. Chang, D. Prezzi, A. Ruini, E. Molinari, M.S. Strano, C. Thomsen, C. Lienau, Phys. Rev. B **72**, 241402(R) (2005); J. Maultzsch, R. Pomraenke, S. Reich, E. Chang, D. Prezzi, A. Ruini, E. Molinari, M.S. Strano, C. Thomsen, C. Lienau, Phys. Rev. B **74**, 169901(2007)
32. Z. Wang, H. Pedrosa, T. Krauss, L. Rothberg, Phys. Rev. Lett. **96**, 047403 (2006)